AIChE

Gas-Solid Flow Distribution through Identical Vertical Passages: Modeling and Stability Analysis

Mohammad S. Masnadi, Siamak Elyasi, John R. Grace, and Xiaotao Bi
Dept. of Chemical and Biological Engineering, University of British Columbia, 2360 East Mall, Vancouver, Canada V6T 1Z3

DOI 10.1002/aic.12131
Published online January 8, 2010 in Wiley InterScience (www.interscience.wiley.com).

As previous evidence shows, the distribution of gas-solid flow traveling through identical parallel paths can be significantly nonuniform, often with harmful operating consequences in practice. A fundamental analytical and numerical study is performed on the distribution of gas-solid pneumatic flow passing through a "Y branch". While many steady-state gas-solid distribution solutions, including a uniform distribution, satisfy the governing equations, linear stability analysis indicates that the uniform distribution is stable the most likely solution of the system. Both 2-D (two-dimensional) and 3-D multiphase computational fluid dynamic simulations and stability analyses confirm the analytical conclusions. © 2010 American Institute of Chemical Engineers *AIChE J,* 56: 2039–2051, 2010

Keywords: multiphase flow, gas-solid systems, maldistribution, bifurcation, stability

Introduction

It is commonly assumed when flow in a single pipe splits symmetrically into several identical branches, that the gas and solids flow in each of the branches will be the same. However, many cases have been found where there is preferential flow, with disproportionate flows in different paths.[1–17] The resulting gas-solid maldistribution may be detrimental in process units, causing such problems as suboptimal overall cyclone efficiency, suboptimal reactor performance, formation of differential erosion and fouling through parallel paths, more frequent shutdowns, suboptimal and unbalanced heat transfer and need for mechanical valve in return lines to control the process. Although a number of studies have been done on gas-liquid flow distribution,[18–20] very few focused and fundamental analyses are available concerning the maldistribution of gas-solid flow passing through identical parallel paths.[10,21] Further study is needed to determine the conditions under which symmetry breaking and flow maldistribution occur.

In some cases, an external cause, such as nonuniform gas-solid "rope" flow in pipes and bends located upstream of a bifurcation, can make the distribution through the parallel paths nonuniform. This is a major problem related to distribution of pulverized fuel through large parallel coal-fired boilers.[14–15,22] Also numerical studies by Schneider et al.[13] showed that upstream nonuniformities can play a significant role in flow distribution through parallel pipes. In another study, Yue et al.[12] reported maldistribution of gas-solids flow through identical multicyclones at the top exit of a CFB boiler. However, they believe that differences in solid fluxes in each circulating loop before entering the cyclones cause maldistribution of flow through parallel cyclones.

On the other hand, Grace et al.[21] introduced a simple model to explain nonuniform distributions reported in literature in cases where the upstream conditions appear to be symmetrical. They showed that uniform and several maldistributed patterns can satisfy the mass balance and pressure balance conditions of the system. They suggest that "energy dissipation minimization" and "hydrodynamic stability" may play important roles in determining the steady-state flow distribution in such systems.

Correspondence concerning this article should be addressed to M. S. Masnadi at s.masnadi@gmail.com.

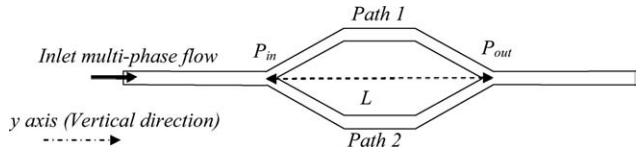

Figure 1. Schematic of two identical vertical parallel paths.

Gas-solid flow maldistribution requires further systematic studies. The objective of this work is to obtain a basic understanding of pneumatic gas-solid flow distribution through identical paths. Pairs of identical pipes and flow symmetry are considered as the reference geometry. The study is intended to provide fundamental insight for flow distribution for very simple geometries involving parallel pipes.

Modeling

For simplicity, we consider vertical pneumatic conveying, where the radial particle concentration distribution is nearly uniform and gas and solids can be reasonably treated as being in 1-D flow.[23]

1-D two-phase flow in a single vertical pipe

Considering an element of length dy of a cylindrical vertical pipe containing a number of solid particles dispersed in a gas, a Lagrangian momentum transfer equations for 1-D flow can be written

$$dm_s \frac{du_s}{dt} = F_{drag} + F_{pressure,s} + F_{gravity,s} + F_{friction,s} \quad (1)$$

$$dm_g \frac{du_g}{dt} = F_{drag} + F_{pressure,g} + F_{gravity,g} + F_{friction,g} \quad (2)$$

where dm_s and dm_g are the masses of particles and fluid, respectively, within the small control volume and u_s and u_g are the solids and gas velocities. Note that the solids drag force acts in the opposite direction on the fluid phase. For this study, the effects of electrostatic forces are ignored. Since the solid density is much greater than that of the gas, the added mass and Basset history terms can be neglected.[24] Also the Saffman shear lift force is neglected. Expressions for each of the differential forces must be supplied to complete the picture. Here we set

$$F_{pressure,s} = (-\frac{dP}{dy})\frac{dm_s}{\rho_s} \quad (3)$$

$$F_{gravity,s} = -dm_s g \quad (4)$$

$$F_{friction,s} = -\frac{2f_s u_s^2 dm_s}{D} \quad (5)$$

where f_s is the solid Fanning friction factor, and D is the pipe inner diameter. Various expressions for the friction factor can be found in the literature.[25] The widely-applied correlation proposed by Konno and Saito[26] is adopted here. For the fluid phase the corresponding equations are

$$F_{pressure,g} = (-\frac{dP}{dy})\frac{dm_g}{\rho_g} \quad (6)$$

$$F_{gravity,g} = -dm_g g \quad (7)$$

$$F_{friction,g} = -\frac{2f_g u_g^2 dm_g}{D} \quad (8)$$

where f_g is the gas Fanning friction factor. In most pneumatic transport systems, the flow is turbulent. A number of different expressions could be used to represent this friction factor. The Koo equation,[27] recommended by Klinzing[28] is used in this study.

The differential masses of particles and fluid can be written, respectively as

$$dm_s = (1-\varepsilon)\rho_s dV = (1-\varepsilon)\rho_s A dy \quad (9)$$

$$dm_g = \varepsilon\rho_g dV = \varepsilon\rho_g A dy \quad (10)$$

where dV is the system differential volume.

Summing Eqs. 1 and 2, and replacing terms by the aforementioned expressions results in the basic dynamic equation for the multiparticle analysis

$$-\int dP = \int \begin{pmatrix} \rho_g \varepsilon g + \rho_s(1-\varepsilon)g + 0.057\sqrt{\frac{g}{D}}\rho_s(1-\varepsilon)u_s + \frac{0.0028\rho_g \varepsilon u_g^2}{D} \\ + \frac{0.25\rho_g^{0.68}\mu^{0.32}\varepsilon u_g^{1.68}}{D^{1.32}} + (1-\varepsilon)\rho_s\frac{du_s}{dt} + \varepsilon\rho_g\frac{du_g}{dt} \end{pmatrix} dy \quad (11)$$

The first two terms on the right side integral are static contributions, whereas the next three are due to wall friction, and the final two terms arise from acceleration. Several other formulations exist to describe the overall dynamic energy loss sum in terms of the pressure drop.[26] Govier and Aziz[29] and Weber[30] used formulations similar to Eq. 11. Equation 11 is used later to study the distribution of gas-solid flow through identical parallel vertical pipes.

1-D two-phase flow in two identical vertical parallel pipes

Extension from a single channel to two vertical identical parallel channels with identical fluid and particle properties, as shown in Figure 1, leads to

$$\frac{-\Delta P_1}{L} = \frac{P_{in} - P_{out}}{L} = \rho_g \varepsilon_1 g + \rho_s(1-\varepsilon_1)g + 0.057\sqrt{\frac{g}{D}}\rho_s (1-\varepsilon_1)u_{s1} + \frac{0.0028\rho_g \varepsilon_1 u_{g1}^2}{D} + \frac{0.25\rho_g^{0.68}\mu^{0.32}\varepsilon_1 u_{g1}^{1.68}}{D^{1.32}} + (1-\varepsilon_1)\rho_s\frac{du_{s1}}{dt} + \varepsilon_1\rho_g\frac{du_{g1}}{dt} \quad (12)$$

$$\frac{-\Delta P_2}{L} = \frac{P_{in} - P_{out}}{L} = \rho_g \varepsilon_2 g + \rho_s(1-\varepsilon_2)g + 0.057\sqrt{\frac{g}{D}}\rho_s(1-\varepsilon_2)u_{s2} + \frac{0.0028\rho_g \varepsilon_2 u_{g2}^2}{D} + \frac{0.25\rho_g^{0.68}\mu^{0.32}\varepsilon_2 u_{g2}^{1.68}}{D^{1.32}} + (1-\varepsilon_2)\rho_s\frac{du_{s2}}{dt} + \varepsilon_2\rho_g\frac{du_{g2}}{dt} \quad (13)$$

Table 1. Defined Operating Conditions (20°C and 101.3 kPa)

Gas	
Type	Air
Density (kg/m^3)	1.225
Viscosity (kg/m.s)	1.79E-05
Inlet velocity (m/s)	20
Solids	
Type	Glass Beads
Density (kg/m^3)	2500
Particle size (μm)	30
Terminal velocity (m/s)	0.68
Volume fraction, α_s (%)=1-α	10

In the aforementioned two equations, it is assumed that the flow is fully developed.

Fully developed steady-state solution

The only criterion of the system is the equality of pressure drops in paths 1 and 2. Therefore, if one considers only the fully developed steady state so that the time-derivative terms are ignored, and assuming equal pressure drop in both channels, i.e., $\Delta P_1 = \Delta P_2$ in Eqs.12 and 13, one obtains

$$\rho_g g(\varepsilon_1 - \varepsilon_2) + \rho_s g(\varepsilon_2 - \varepsilon_1) + 0.057\sqrt{\frac{g}{D}}\rho_s(u_{s1}(1-\varepsilon_1) - u_{s2}(1-\varepsilon_2)) + \frac{0.0028\rho_g}{D}(\varepsilon_1 u_{g1}^2 - \varepsilon_2 u_{g2}^2) + \frac{0.25\rho_g^{0.68}\mu^{0.32}}{D^{1.32}}(\varepsilon_1 u_{g1}^{1.68} - \varepsilon_2 u_{g2}^{1.68}) = 0 \quad (14)$$

In addition, gas and solids continuity give volumetric flow rates of

$$Q_{g1} = \gamma Q_{gt} = A\varepsilon_1 u_{g1} \quad (15)$$

$$Q_{g2} = (1-\gamma)Q_{gt} = A\varepsilon_2 u_{g2} \quad (16)$$

$$Q_{s1} = \sigma Q_{st} = A(1-\varepsilon_1)u_{s1} \quad (17)$$

$$Q_{s2} = (1-\sigma)Q_{st} = A(1-\varepsilon_2)u_{s2} \quad (18)$$

where γ and σ are the fractions of the gas and solids flows, respectively, passing through channel 1. Note that for a uniform distribution of gas and solids $\gamma = \sigma = 0.5$.

Yang[31] proposed an implicit correlation for estimating particle velocity. Applying this to both paths yields

$$u_{s1} = u_{g1} - u_t\left(1 + \frac{0.057 u_{s1}\varepsilon_1^{4.7}}{\sqrt{gD}}\right)^{0.5} \quad (19)$$

$$u_{s2} = u_{g2} - u_t\left(1 + \frac{0.057 u_{s2}\varepsilon_2^{4.7}}{\sqrt{gD}}\right)^{0.5} \quad (20)$$

where u_t is the single particle terminal velocity in undisturbed gas of identical properties.

Equations 14 to 20 constitute seven nonlinear algebraic equations, but there are eight unknowns (γ, σ, u_{g1}, u_{s1}, ε_1, u_{g2}, u_{s2} and ε_2). Hence, for two parallel paths, there is one extra degree of freedom, unless we can invoke an extra condition, such as pressure drop minimization.[10,21] Note, however, that the uniform condition (where $\gamma = \sigma = 0.5$; $u_{g1} = u_{g2}$; $u_{s1} = u_{s2}$; and $\varepsilon_1 = \varepsilon_2$) satisfies all seven equations, and, hence, always represents one solution. Whether this solution is stable or unstable is considered below.

Solution for one case study

To solve Eqs. 14 to 20, γ is chosen as the variable to be specified. We are then left with seven nonlinear algebraic equations and seven unknowns. A vertical cylindrical pipe is selected with an overall height of 610 mm and a diameter of 38 mm. Other operating conditions are summarized in Table 1. The terminal velocity was calculated using the drag coefficient empirical expression proposed by Wang et al.[32]

Figures 2 to 5 represent steady-state solutions for flow through two vertical identical parallel pipes symmetrically connected to a entry pipe by "Y". Figure 2 shows all gas and solid distribution solutions. Note that in addition to equal distribution of gas-solid flow through the parallel paths, many nonuniform distributions (σ and $\gamma \neq 0.5$) of multiphase flow through the different branches satisfy the pressure drop and continuity requirements. There is no solution for γ equal to 0 or 1. Physically, in these two conditions, one of the paths will contain no gas (so there will be no pressure drop), and, consequently, the entire gas flow will pass through the other branch (resulting in a pressure drop in that path). Therefore, the pressure balance criterion cannot be satisfied.

Figure 3 shows the effect of unequal distribution of gas-solid flow on the pressure drop of the system. In this case, the uniform distribution with exactly half the gas and half the solids passing through each path gives the lowest pressure drop. It has been argued[33] that flowing physical systems are likely to approach an extremum in practice, where they, for example, minimize or maximize the rate of dissipation of potential energy. Based on this premise, it may be that the energy dissipation minimization case, i.e., the uniform gas-solid distribution solution consuming minimum energy, is the most likely solution for the system. Note, however, that, although the maldistribution of phases results in more energy dissipation (higher pressure drop) for the system, the

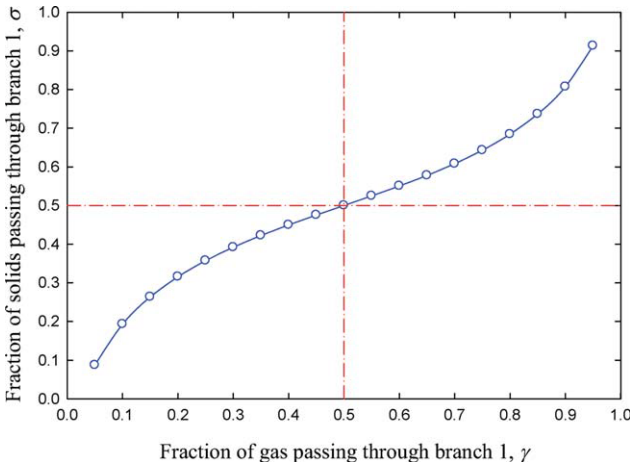

Figure 2. Relationship between gas and solids distribution parameters for steady-state solutions.

[Color figure can be viewed in the online issue, which is available at www.interscience.wiley.com.]

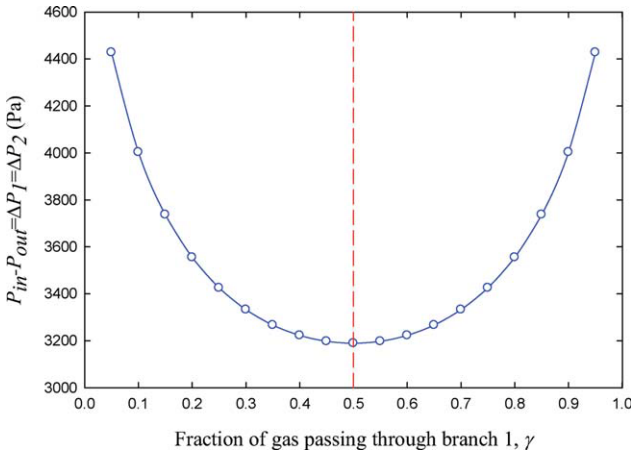

Figure 3. Effect of mal-distribution on pressure drop of the system.

[Color figure can be viewed in the online issue, which is available at www.interscience.wiley.com.]

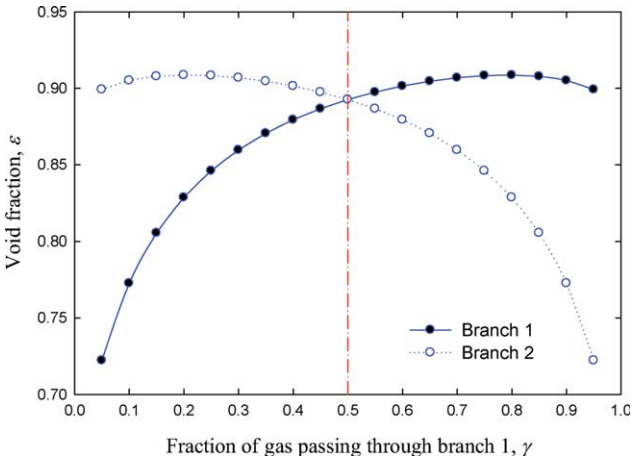

Figure 5. Voidage distribution pattern.

[Color figure can be viewed in the online issue, which is available at www.interscience.wiley.com.]

pressure drop difference between the uniform distribution and nonuniform solutions is small. For example, the difference between the pressure drops for the uniform distribution ($\gamma = 0.5$) and the $\gamma = 0.7$ solution is only 4.5%.

Figure 2 shows that when more gas passes through path 1, equality of pressure drops requires that more solids enter the same branch. Based on Figure 4, the branch with more gas and solids flow also has higher gas and solid velocities than the branch with the lower flow. Figure 5 helps to explain how the system can provide equal pressure drop in both branches when more gas and more solids flow through the same branch. Consider the case where more gas and solids passes through branch 1 (i.e., γ and σ are both > 0.5). From Figure 5, by going far from equal distribution point (to the right from $\gamma = 0.5$), the voidage in branch 1 increases, whereas that in branch 2 decreases more steeply. To maintain the pressure drops in balance, the line with less gas and solids flow (branch 2) adopts a lower void fraction, causing enough extra hydrostatic pressure drop to compensate for the higher velocities and flow rates, and, hence, the higher frictional losses, in branch 1.

1-D two-phase flow in N identical vertical parallel pipes

Extension of Eq. 11 leads to an equation of motion for each of N vertical identical pipes in parallel. Based on the same approach as above, the system of equations for the steady-state motion of gas-solid flow through N parallel paths is summarized in Table 2. Based on the analysis of Grace,[10] the two-phase system with N parallel paths has (N+1) degrees of freedom. Again an equal distribution of solids and gas for each of the N paths clearly satisfies all the equations, but this situation is not unique for N≥2.

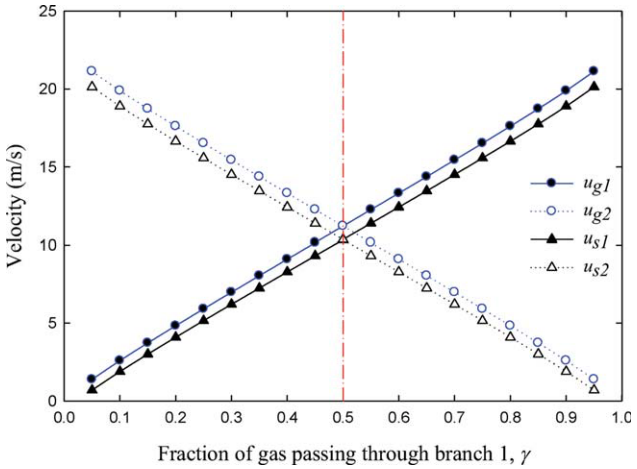

Figure 4. Path 1 and 2 gas and solid velocities for several gas distribution solutions.

[Color figure can be viewed in the online issue, which is available at www.interscience.wiley.com.]

Table 2. System of Equations for Distribution of Gas-Solid through *N* Parallel Paths

Expression	Equation No
$\rho_g g(\varepsilon_1 - \varepsilon_2 - \cdots - \varepsilon_N) + \rho_s g(\varepsilon_N - \varepsilon_{N-1} - \cdots - \varepsilon_1)$ $+ 0.057\sqrt{\frac{g}{D}}\rho_s(u_{s1}(1-\varepsilon_1) - u_{s2}(1-\varepsilon_2) - \cdots - u_{sN}(1-\varepsilon_N))$ $+ \frac{0.0028\rho_g}{D}(\varepsilon_1 u_{g1}^2 - \varepsilon_2 u_{g2}^2 - \cdots - \varepsilon_N u_{gN}^2)$ $+ \frac{0.25\rho_g^{0.68}\mu^{0.32}}{D^{1.32}}(\varepsilon_1 u_{g1}^{1.68} - \varepsilon_2 u_{g2}^{1.68} - \cdots - \varepsilon_N u_{gN}^{1.68}) = 0$	(21)
$Q_{gi} = \gamma_i Q_{gt} = A\varepsilon_i u_{gi}, \quad i = 1, \ldots, N$	(22)
$Q_{si} = \sigma_i Q_{st} = A(1-\varepsilon_i)u_{si}, \quad i = 1, \ldots, N$	(23)
$u_{si} = u_{gi} - u_t\left(1 + \frac{0.057 u_{si}\varepsilon_i^{4.7}}{\sqrt{gD}}\right)^{0.5}, \quad i = 1, \ldots, N$	(24)

Stability Analysis

Linearized stability analysis involves study of the response of a system to a small perturbation to see whether it grows, remains unchanged or decreases with time. A linear stability analysis is next performed on the steady-state solution for $N = 2$.

Linear stability analysis for a single pipe

For 1-D gas and solids flow we have

$$Q_g = u_g A\varepsilon \tag{25}$$

$$Q_s = u_s A(1-\varepsilon) \tag{26}$$

We can also write

$$Q_g = kQ_s \tag{27}$$

where k is a flow coefficient. From the aforementioned expressions, it is possible to rearrange Eq. 11 as a function of solids flow rate. Applying the chain rule for the time-dependent terms of Eq. 11 and after substitution, the final expression for the pressure drop of a single vertical pipe as a function of solid flow rate is

$$\frac{-\Delta P}{L} = \frac{P_{in} - P_{out}}{L} = f(Q_s,\varepsilon,k) + \left(\frac{\rho_s + \rho_g k}{A}\right)\frac{dQ_s}{dt} + \left(\frac{\rho_s Q_s}{A(1-\varepsilon)} - \frac{\rho_g k Q_s}{A\varepsilon}\right)\frac{d\varepsilon}{dt} + \frac{\rho_g Q_s}{A}\frac{dk}{dt} \tag{28}$$

where $f(Q_s, \varepsilon, k)$ is given by

$$f(Q_s,\varepsilon,k) = \rho_g \varepsilon g + \rho_s(1-\varepsilon)g + 0.057\sqrt{\frac{g}{D}}\frac{\rho_s}{A}Q_s + \frac{0.0028\rho_g k^2 Q_s^2}{DA^2\varepsilon} + \frac{0.25\mathrm{Re}^{-0.32}\rho_g k^2 Q_s^2}{DA^2\varepsilon} \tag{29}$$

Introducing a small perturbation in the solid-flow rate q_s, around the steady-state solution $Q_{s,\ \mathrm{steady}}$, and applying Taylor expansion for each term yields

$$P_{in} = P_{in,steady} + \frac{dP_{in}}{dQ_s}q_s \tag{30}$$

$$f(Q_s,\varepsilon,k) = f_{steady}(Q_s,\varepsilon,k) + \frac{df(Q_s,\varepsilon,k)}{dQ_s}q_s \tag{31}$$

$$\frac{dQ_s}{dt} = \frac{d(Q_{s,steady} + q_s)}{dt} = \frac{dq_s}{dt} \tag{32}$$

$$\frac{d\varepsilon}{dt} = \frac{d(\varepsilon_{steady} + \frac{d\varepsilon}{dQ_s}q_s)}{dt} = \frac{d\varepsilon}{dQ_s}\frac{dq_s}{dt} \tag{33}$$

$$\frac{dk}{dt} = \frac{d(k_{steady} + \frac{dk}{dQ_s}q_s)}{dt} = \frac{dk}{dQ_s}\frac{dq_s}{dt} \tag{34}$$

Here $P_{\mathrm{in,\ steady}}$, f_{steady} $(Q_s,\ \varepsilon,\ k)$, $Q_{\mathrm{s,\ steady}}$, $\varepsilon_{\mathrm{steady}}$ and k_{steady} are the corresponding steady-state parameters. It is assumed that the effect of solid perturbation on the outlet pressure is negligible. After substitution of Taylor expanded terms into Eq. 28, we obtain the following equation for the perturbation variable q_s

$$\frac{1}{L}\frac{dP_{in}}{dQ_s}q_s = \frac{df(Q_s,\varepsilon,k)}{dQ_s}q_s + T\frac{dq_s}{dt} \tag{35}$$

where

$$T = \left[\left(\frac{\rho_s + \rho_g k}{A}\right) + \left(\left(\frac{\rho_s Q_s}{A(1-\varepsilon)} - \frac{\rho_g k Q_s}{A\varepsilon}\right)\frac{d\varepsilon}{dQ_s}\right) + \left(\left(\frac{\rho_g Q_s}{A}\right)\frac{dk}{dQ_s}\right)\right] \tag{36}$$

An exponential model is considered for the perturbation parameter so that

$$q_s = \delta_s e^{\lambda t} \tag{37}$$

where δ_s is the perturbation amplitude, and λ is an eigenvalue or growth factor. The sign of λ determines the stability of solution. For $\lambda \leq 0$, the solution is stable and the perturbation term shrinks and disappears as time passes. A more negative value of λ causes faster disappearance of the perturbation. On the other hand, for $\lambda > 0$, q_s grows exponentially and the solution is unstable.

Substituting Eq. 37 into 35 and solving for the eigenvalue yields

$$\lambda = \frac{\frac{dP_{in}}{dQ_s} - L\frac{df(Q_s,\varepsilon,k)}{dQ_s}}{LT} \tag{38}$$

For this case study, T is greater than zero. The condition for stability, $\lambda \leq 0$, therefore, requires that

$$\frac{dP_{in}}{dQ_s} \leq L\frac{df(Q_s,\varepsilon,k)}{dQ_s} \tag{39}$$

Based on Eq. 28 since $f\ (Q_s,\ \varepsilon,\ k)$ is equal to the steady-state pressure drop of the system divided by L, the aforementioned condition is always satisfied for a single pipe, and the system is always stable.

Linear stability analysis for two identical vertical parallel pipes

A similar approach is followed for two identical parallel paths. Based on Eqs.12 and 13, considering two vertical pipes and perturbing the solid flow rates yield

$$\frac{dP_{in}}{dQ_{st}}(q_{s1} + q_{s2}) - L\frac{df_1(Q_{s1},\varepsilon_1,k_1)}{dQ_{s1}}q_{s1} - LT_1\frac{dq_{s1}}{dt} = 0 \tag{40}$$

$$\frac{dP_{in}}{dQ_{st}}(q_{s1} + q_{s2}) - L\frac{df_2(Q_{s2},\varepsilon_2,k_2)}{dQ_{s2}}q_{s2} - LT_2\frac{dq_{s2}}{dt} = 0 \tag{41}$$

where

$$T_1 = \left[\left(\frac{\rho_s + \rho_g k_1}{A} \right) + \left(\left(\frac{\rho_s Q_{s1}}{A(1-\varepsilon_1)} - \frac{\rho_g k_1 Q_{s1}}{A\varepsilon_1} \right) \frac{d\varepsilon_1}{dQ_{s1}} \right) + \left(\left(\frac{\rho_g Q_{s1}}{A} \right) \frac{dk_1}{dQ_{s1}} \right) \right] \quad (42)$$

$$T_2 = \left[\left(\frac{\rho_s + \rho_g k_2}{A} \right) + \left(\left(\frac{\rho_s Q_{s2}}{A(1-\varepsilon_2)} - \frac{\rho_g k_2 Q_{s2}}{A\varepsilon_2} \right) \frac{d\varepsilon_2}{dQ_{s2}} \right) + \left(\left(\frac{\rho_g Q_{s2}}{A} \right) \frac{dk_2}{dQ_{s2}} \right) \right] \quad (43)$$

$$f_1(Q_{s1}, \varepsilon_1, k_1) = \rho_g \varepsilon_1 g + \rho_s (1-\varepsilon_1) g + 0.057 \sqrt{\frac{g}{D}} \frac{\rho_s}{A} Q_{s1} + \frac{0.0028 \rho_g k_1^2 Q_{s1}^2}{DA^2 \varepsilon_1} + \frac{0.25 \mathrm{Re}_1^{-0.32} \rho_g k_1^2 Q_{s1}^2}{DA^2 \varepsilon_1} \quad (44)$$

$$f_2(Q_{s2}, \varepsilon_2, k_2) = \rho_g \varepsilon_2 g + \rho_s (1-\varepsilon_2) g + 0.057 \sqrt{\frac{g}{D}} \frac{\rho_s}{A} Q_{s2} + \frac{0.0028 \rho_g k_2^2 Q_{s2}^2}{DA^2 \varepsilon_2} + \frac{0.25 \mathrm{Re}_2^{-0.32} \rho_g k_2^2 Q_{s2}^2}{DA^2 \varepsilon_2} \quad (45)$$

Likewise for perturbation variables q_{s1} and q_{s2}, we have

$$q_{s1} = \delta_{s1} e^{\lambda t} \quad (46)$$

$$q_{s2} = \delta_{s2} e^{\lambda t} \quad (47)$$

where $q_s = q_{s1} + q_{s2}$. Substitution of Eqs. 46 and 47 into 40 and 41 yields

$$\frac{dP_{in}}{dQ_{st}} (\delta_{s1} + \delta_{s2}) - L \frac{df_1(Q_{s1}, \varepsilon_1, k_1)}{dQ_{s1}} \delta_{s1} - LT_1 \lambda \delta_{s1} = 0 \quad (48)$$

$$\frac{dP_{in}}{dQ_{st}} (\delta_{s1} + \delta_{s2}) - L \frac{df_2(Q_{s2}, \varepsilon_2, k_2)}{dQ_{s2}} \delta_{s2} - LT_2 \lambda \delta_{s2} = 0 \quad (49)$$

The system would again be stable if $\lambda \leq 0$. The eigenvalues are solutions of the following determinant, or second-order characteristic polynomial

$$\begin{vmatrix} \frac{dP_{in}}{dQ_{st}} - L \frac{df_1(Q_{s1}, \varepsilon_1, k_1)}{dQ_{s1}} - LT_1 \lambda & \frac{dP_{in}}{dQ_{st}} \\ \frac{dP_{in}}{dQ_{st}} & \frac{dP_{in}}{dQ_{st}} - L \frac{df_2(Q_{s2}, \varepsilon_2, k_2)}{dQ_{s2}} - LT_2 \lambda \end{vmatrix} = 0 \quad (50)$$

$$a_2 \lambda^2 + a_1 \lambda + a_0 = 0 \quad (51)$$

where

$$a_2 = L^2 T_1 T_2 \quad (52)$$

$$a_1 = \left(L^2 \frac{df_1}{dQ_{s1}} - L \frac{dP_{in}}{dQ_{st}} \right) T_2 + \left(L^2 \frac{df_2}{dQ_{s2}} - L \frac{dP_{in}}{dQ_{st}} \right) T_1 \quad (53)$$

$$a_0 = -L \frac{dP_{in}}{dQ_{st}} \left(\frac{df_1}{dQ_{s1}} + \frac{df_2}{dQ_{s2}} \right) + L^2 \left(\frac{df_1}{dQ_{s1}} \cdot \frac{df_2}{dQ_{s2}} \right) \quad (54)$$

The Routh-Hurwitz stability criterion is used to find the sign of the eigenvalues. The corresponding Routh-Hurwitz table is

$$\begin{vmatrix} a_2 & a_0 \\ a_1 & 0 \\ a_0 & 0 \end{vmatrix} \quad (55)$$

For the case study with operating conditions presented in Table 1, both T_1 and T_2 are greater than zero. Also, since the total input gas and solids flow rates are constant, $dP_{in}/dQ_{st} \rightarrow -\infty$ at the limit. (Pustylnik et al.[34] reached the same result for a gas-liquid system. Detailed calculations are available elsewhere[35]). Hence, for all steady-state solutions, a_2 and a_1 are always greater than zero. Therefore, the sign of a_0 determines whether or not the system is stable. Hence, for each steady-state solution, if the sign of a_0 is positive, all corresponding eigenvalues are less than zero and the system is stable.

From Eqs. 28 and 29, it can be understood that $\Delta P_i = L.f_i(Q_{si}, \varepsilon_i, k_i)$. Therefore, for two parallel paths, *Total pressure drop* $= \Delta P_1 = \Delta P_2 = L.f_1(Q_{s1}, \varepsilon_1, k_1) = L.f_2(Q_{s2}, \varepsilon_2, k_2)$. Thus, it can be shown easily that

$$\frac{d(Total\ pressure\ drop)}{dQ_{s1}} = L \frac{df_1(Q_{s1}, \varepsilon_1, k_1)}{dQ_{s1}} \quad (56)$$

$$\frac{d(Total\ pressure\ drop)}{dQ_{s2}} = L \frac{df_2(Q_{s2}, \varepsilon_2, k_2)}{dQ_{s2}} \quad (57)$$

Figure 6 shows the steady-state total pressure drop for the conditions defined in Table 1 as a function of solid flow rates through paths 1 and 2. Because of the symmetry of the system, the mirror projection of a data point in path 1 has a corresponding point in path 2. For example, "Point A" in Figure 6 for path 1 has a related point in path 2 of "Point B". Paths 1 and 2 share a common region at the "uniform distribution" point. It can be easily shown that for the entire maldistributed steady-state solutions, $df_1/dQ_{s1} = -df_2/dQ_{s2}$,

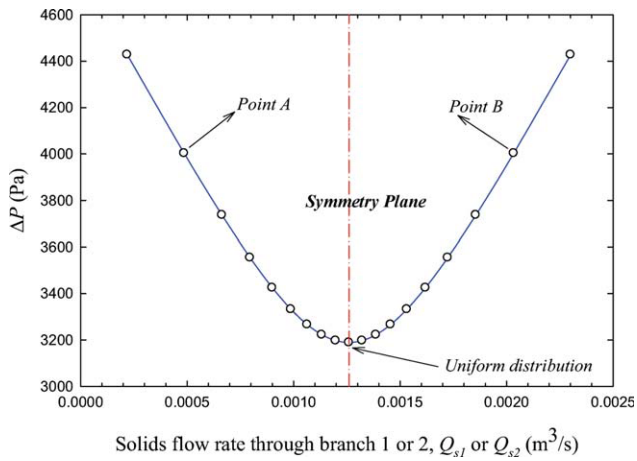

Figure 6. Pressure drop as a function of solid flow rates through paths 1 and 2 for a system whose properties are given in Table 1.

[Color figure can be viewed in the online issue, which is available at www.interscience.wiley.com.]

whereas for the uniform steady-state solution, $df_1/dQ_{s1} = df_2/dQ_{s2} = 0$.

Therefore, for the maldistributed solutions ($\gamma \neq 0.5$), the first term of Eq. 54 is zero. Also because of the symmetry in Figure 6, the second term of a_0 is always negative, and, thus, $a_{0,\text{ unequal distribution}} < 0$. Therefore, all unequal steady-state solutions for the case study are unstable.

On the other hand, for the uniform distribution solution ($\gamma = 0.5$), both the first and second terms of Eq. 54 are zero, and, therefore, $a_{0,\text{ equal distribution}} = 0$. Thus, from Eq. 51, the uniform distribution eigenvalues are $\lambda_{1,\text{ equal distribution}} = 0$ and $\lambda_{2,\text{ unequal distribution}} = -a_1/a_2 < 0$. Therefore, the uniform distribution of gas-solid flow is the only stable case among all the steady-state solutions.

Stability analysis for N identical vertical parallel pipes

Once steady-state solutions are obtained, the stability of the solutions is analyzed using Eq. 35 for each path

$$\frac{dP_{in}}{dQ_{st}}(q_{s1} + ... + q_{sN}) - L\frac{df_i(Q_{si}, \varepsilon_i, k_i)}{dQ_{si}}q_{si} - LT_i\frac{dq_{si}}{dt} = 0, \quad i = 1...N \tag{58}$$

where

$$T_i = \left[\left(\frac{\rho_s + \rho_g k_i}{A}\right) + \left(\left(\frac{\rho_s Q_{si}}{A(1-\varepsilon_i)} - \frac{\rho_g k_i Q_{si}}{A\varepsilon_i}\right)\frac{d\varepsilon_i}{dQ_{si}}\right) + \left(\left(\frac{\rho_g Q_{si}}{A}\right)\frac{dk_i}{dQ_{si}}\right)\right], \quad i = 1...N \tag{59}$$

$$f_i(Q_{si}, \varepsilon_i, k_i) = \rho_g \varepsilon_i g + \rho_s(1-\varepsilon_i)g + 0.057\sqrt{\frac{g}{D}}\frac{\rho_s}{A}Q_{si} + \frac{0.0028\rho_g k_i^2 Q_{si}^2}{DA^2\varepsilon_i} + \frac{0.25\mathrm{Re}_i^{-0.32}\rho_g k_i^2 Q_{si}^2}{DA^2\varepsilon_i}, \quad i = 1...N \tag{60}$$

Substituting $\delta_{si}e^{\lambda t}$ for perturbation variables (q_{si}) yields

$$\frac{dP_{in}}{dQ_{st}}(\delta_{s1} + ... + \delta_{sN}) - L\frac{df_i(Q_{si}, \varepsilon_i, k_i)}{dQ_{si}}\delta_{si} - LT_i\lambda\delta_{si} = 0, \quad i = 1...N \tag{61}$$

The system is stable for $\lambda \leq 0$. The eigenvalue is a solution of the characteristic polynomial

$$a_i\lambda^i + a_{i-1}\lambda^{i-1} + ... + a_1\lambda + a_0 = 0, \quad i = 1...N \tag{62}$$

that is the simplified form of determinant

$$\begin{bmatrix} \frac{dP_{in}}{dQ_{st}} - \frac{df_1}{dQ_{s1}} - LT_1\lambda & \cdots & \frac{dP_{in}}{dQ_{st}} \\ \frac{dP_{in}}{dQ_{st}} & \frac{dP_{in}}{dQ_{st}} - \frac{df_2}{dQ_{s2}} - LT_2\lambda & \frac{dP_{in}}{dQ_{st}} \\ \cdots & \cdots & \cdots \\ \frac{dP_{in}}{dQ_{st}} & \cdots & \frac{dP_{in}}{dQ_{st}} - \frac{df_N}{dQ_{sN}} - LT_N\lambda \end{bmatrix} \begin{bmatrix} \delta_1 \\ \delta_2 \\ \cdot \\ \cdot \\ \cdot \\ \cdot \\ \delta_N \end{bmatrix} = 0 \tag{63}$$

Again the sign of the eigenvalues, roots of Eq. 62, can be determined using the Routh-Hurwitz stability criterion.

From Eq. 60, considering an even distribution solution for N paths, it is easily proven that

$$f_1(Q_{s_1}) = f_2(Q_{s_2}) = ... = f_N(Q_{sN}) \tag{64}$$

$$T_1 = T_2 = ... = T_N \tag{65}$$

Therefore, by considering the aforementioned relationship in expression (63), the following eigenvalues can be obtained

$$\begin{cases} \lambda_1 = \frac{N\frac{dP_{in}}{dQ_{st}} - L\frac{df_i}{dQ_{si}}}{LT}, & i = 2...N \\ \lambda_i = \frac{-\frac{df_i}{dQ_{si}}}{2T} \end{cases} \tag{66}$$

For cases where $T > 0$, the condition of stability is satisfied if all eigenvalues are equal or less than zero; i.e.

$$\begin{cases} N\frac{dP_{in}}{dQ_{st}} - L\frac{df_i}{dQ_{si}} \leq 0, & i = 2...N \\ -\frac{df_i}{dQ_{si}} \leq 0 \end{cases} \tag{67}$$

Since the inlet total solid flow rate is constant, dP_{in}/dQ_{st} approaches $-\infty$, and the first stability condition is always satisfied. Thus, the only condition for stability of the uniform distribution solution for N parallel paths is

$$-\frac{df_i}{dQ_{si}} \leq 0, \quad i = 1...N \tag{68}$$

For example, for the already-discussed two ($N = 2$) parallel pipes, with T_1 and T_2 both >0, $-df_1/dQ_{s1} = -df_2/dQ_s2 = 0$. Therefore, the aforementioned general approach again leads to the uniform distribution solution being the stable solution, consistent with the Routh-Hurwitz stability criterion method.

Discussion of analytical studies

It has been demonstrated that several steady-state gas-solid distribution solutions including the uniform distribution can satisfy the continuity and pressure-drop balance conditions. However, when a perturbation is imposed, for one defined case study, the stability analysis shows that the only steady-state stable solution is the uniformly distributed one, with all maldistributed solutions being unstable. One can question,

based on the proposed model, whether there may be other cases where the uniform distribution solution is unstable or whether some maldistributed solutions are stable? Based on the symmetric behavior of the system about the uniform distribution solution, (e.g., see Figure 3 or Figure 6), any maldistributed solution can be stable if and only if the corresponding data point in its "pressure drop vs. solid flow rate" plot has zero slope (d (*Total pressure drop*)$/dQ_{si} = df_i$ (Q_{si}, ε_i, k_i)$/dQ_{si} = 0$). In other words, the only solutions that are stable are ones where the local or general pressure drop reaches a minimum or maximum. This is perfectly consistent with the energy dissipation optimization approach proposed by Li and Kwauk.[33]

When parametric studies were performed for the same configuration, but different operating conditions (e.g., solid concentration, inlet velocity, etc) and physical dimensions, it was found in all cases that the only stable solution corresponds to the pressure drop reaching a minimum, and that this only occurred for the uniform distribution solution with the geometry considered here. Thus, it is appears that uniformity is favored for different operating conditions and dimensions for gas-solid flow through identical vertical parallel paths.

Numerical Simulation

Although a 1-D model is an acceptable approach for simulating flow of gas-solids suspensions through vertical pipes, it is of interest to study the behavior of the system in 2-D and 3-D space using computational fluid dynamics. FLUENT 6.2 software was used in this regard based on the Euler-Euler approach. Again particle lift forces were ignored compared to drag forces. Also the virtual mass force was neglected, since the solids density is much greater than that of the gas. Based on the solid concentration of the system (~10%), the Gidaspow[36] model was used for interphase momentum exchange coefficient. Also the k-ε model for each phase was chosen to describe the effect of turbulent velocity fluctuations.

2-D simulation

2-D CFD modeling was performed on a vertical "Y branch" geometry, as shown in Figure 7. To compare the numerical results with the analytical ones, all conditions were chosen to be the same as for the analytical case (i.e., Table 1) except that the solids inlet velocity was specified (as 20 m/s) rather than setting the terminal settling velocity. As indicated in Figure 7, gas-solid flow is introduced to the system from the inlet located below the bifurcation. After splitting the multiphase flow, recombination pipes bring the parallel paths together again, and the total flow exits from the outlet section. CFD runs showed that the interactions between two parallel streams at the recombination section may cause local turbulence, increasing the number of iterations needed to achieve convergence. Therefore, as indicated in Figure 7, a small infinitesimally thin symmetric baffle was added to reduce remixing at the recombination.

The geometry was meshed with 46,080 quadrilateral cells. To check the equality of the geometry and meshed cells on the right- and left-hand sides, single-phase flow (air) was passed through the system, and it was confirmed that the flow distributed uniformly through the two paths.

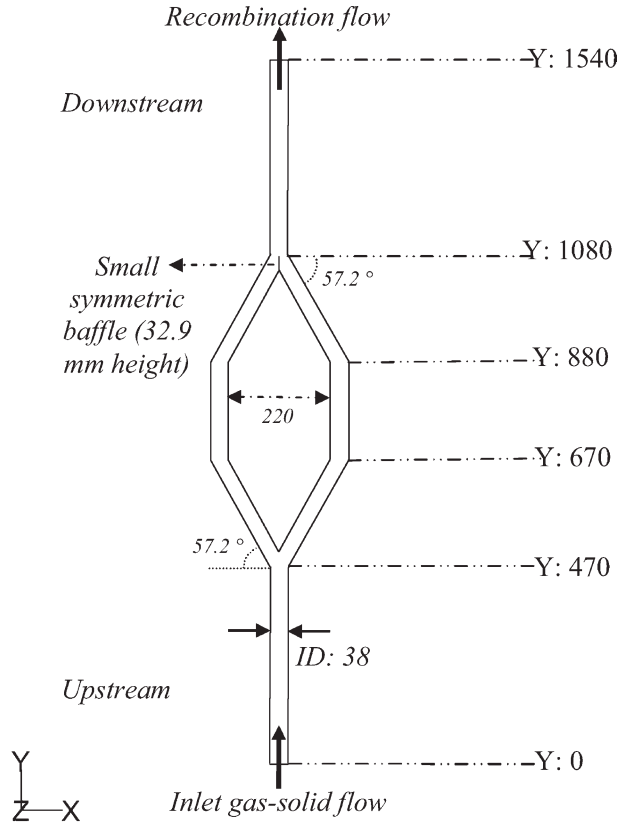

Figure 7. Schematic of 2-D "Y branch" geometry (all dimensions in mm).

Steady-state numerical modeling was performed to investigate gas-solid flow through vertical parallel paths. Two criteria can be used to establish that a solution has been obtained: Magnitude of residuals of different elements decreasing below some preset value, and satisfaction of mass conservation. It should be noted that in many steady-state CFD studies, the residuals are acceptable (e.g., less than 1E-4.0), but since the net mass flow rate (difference between outlet and inlet multiphase flow rates) is far from zero, the iterations should continue until the net flow is very nearly 0.

All of the residuals in this case study were less than 1E-4.0 after 20,000 iterations. However, as shown in Figure 8, up to 30,000 iterations, conservation of mass for the steady-state case was not well satisfied. Even after 30,000 iterations, the inset plot on Figure 8 shows that the oscillations near zero continued. The following results were, therefore, obtained after 90,000 iterations. Figure 9 shows the area-weighted volume fraction as a function of numerical iteration for the left and right vertical pipes. It is clear that by extending the numerical computation, both values approach each other and the uniform distribution is the solution of the simulation.

Figure 10 shows the gas-volume fraction and gas-velocity magnitude through the parallel paths. The distribution of gas flow is uniform, with no discrepancy visible. Figure 11 plots the distribution of solid-volume fraction through the identical parallel paths. The distribution of particles through the vertical "Y branch" is clearly uniform. Also the solid velocity is virtually identical between the left and right pipes. In both cases

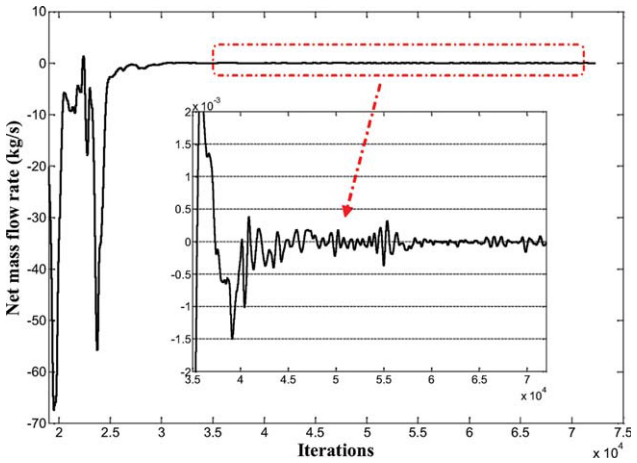

Figure 8. Approach of net mass flow rate to zero.

[Color figure can be viewed in the online issue, which is available at www.interscience.wiley.com.]

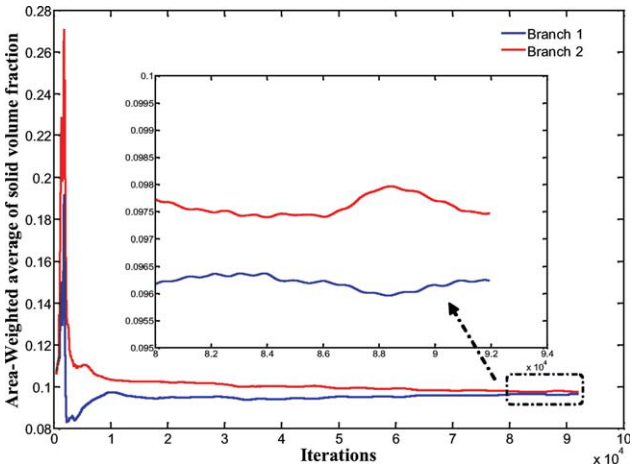

Figure 9. Solid-volume fraction approach for right and left paths vs. numerical iterations.

[Color figure can be viewed in the online issue, which is available at www.interscience.wiley.com.]

the effect of the small interface wall located at the recombination section on preventing the formation of local turbulence between the right and left streams is notable. It should be mentioned that the total pressure drop calculated numerically through the vertical parallel path is 3476 Pa, within 8.3% of the analytical estimation of the pressure drop of the uniform distribution solution in previous section of 3189 Pa.

3-D simulation

The geometry related to 3-D simulation of solids suspension passing through identical parallel branches is demonstrated in Figure 12. The geometry was meshed with 605,172 quadrilateral and 196,768 hexahedral cells. As for

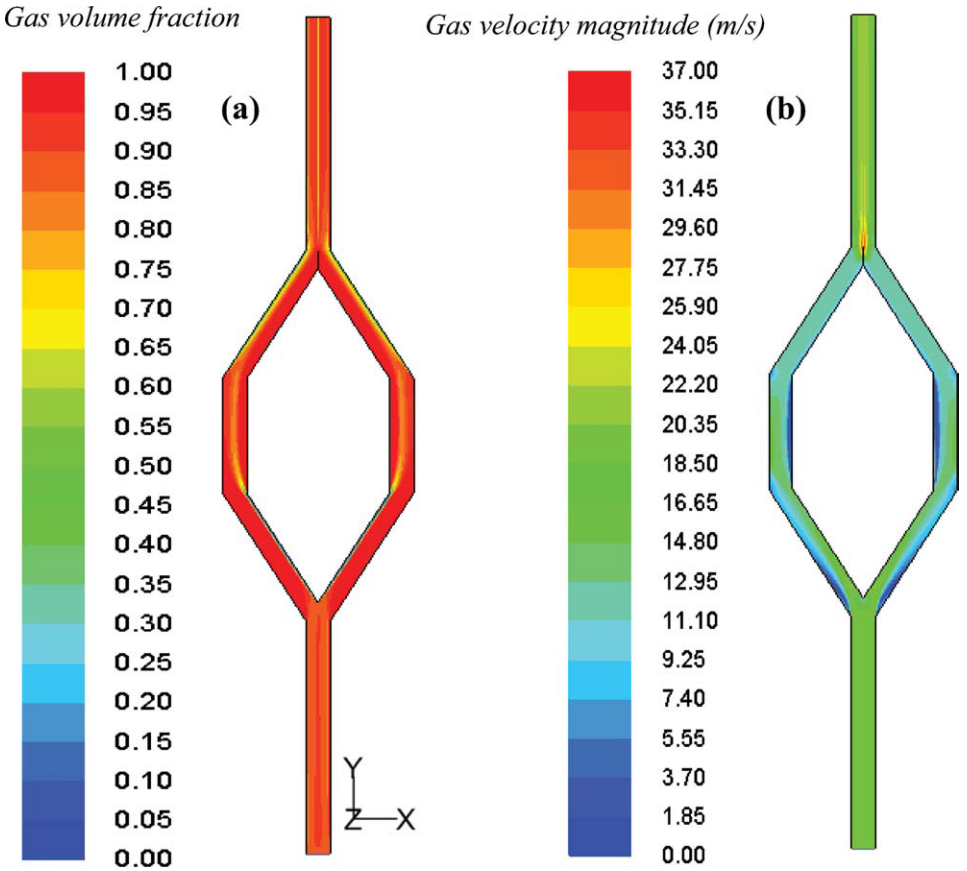

Figure 10. Contours of (a) gas-volume fraction, and (b) gas-velocity magnitude.

[Color figure can be viewed in the online issue, which is available at www.interscience.wiley.com.]

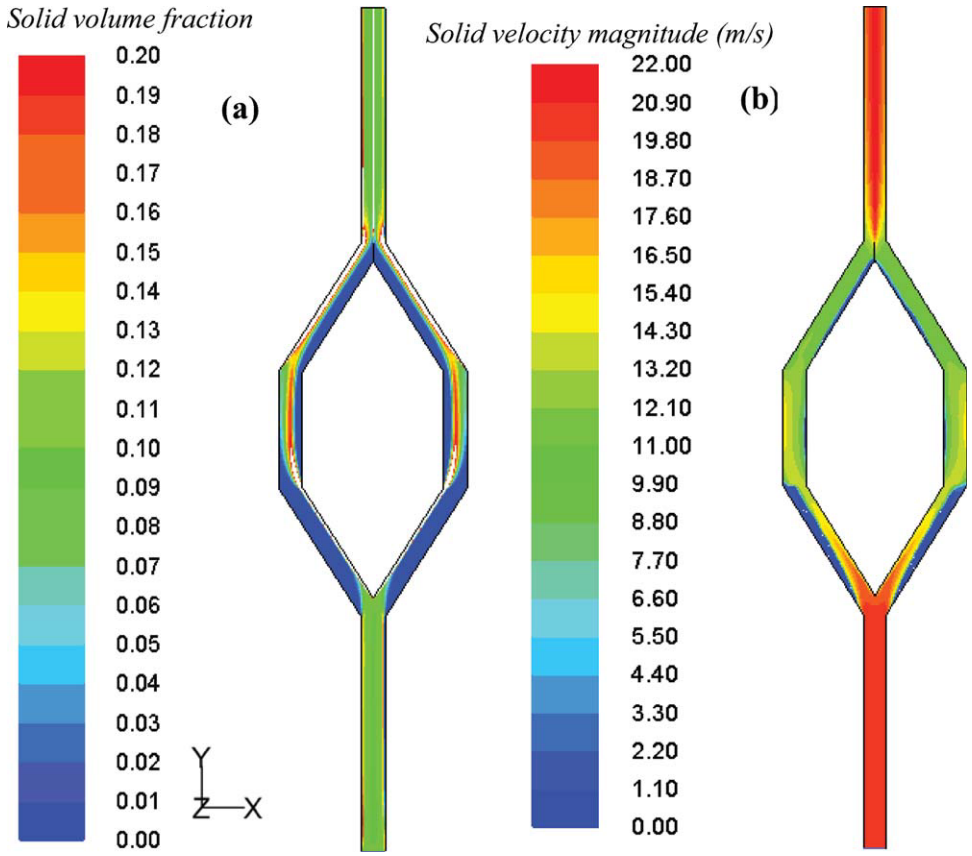

Figure 11. Contours of (a) solid-volume fraction, and (b) solid-velocity magnitude.

White color corresponds to volume fractions > 0.2. [Color figure can be viewed in the online issue, which is available at www.interscience.wiley.com.]

the 2-D case, it was first confirmed that when air was passed through the system, the flow distributed uniformly between the two paths.

The operating conditions were the same as for the 2-D simulation. Convergence was deemed to have been reached after 290,000 iterations. Figure 13 corresponds to the distribution of solid-volume fraction through the geometry. As expected, the solids concentration is higher in the bends. As shown in Figure 14, the steady-state distribution of particles through the vertical "Y branch" is almost uniform. Also the gas is separated uniformly through the parallel pipes as demonstrated in Figure 15. The 3-D results are perfectly consistent with the 2-D simulation.

Numerical stability analysis

Two- and three-dimensional CFD studies again indicated that the gas-solid flow distributed uniformly through the identical parallel paths. As for the analytical approach, the next step was to test the numerical stability of the uniform solution. Considering steady-state condition, solids flow was perturbed. To perturb the system, two methods were used: (a) the system was perturbed by adding some solids with 20 m/s initial velocity to one of the two paths. This was done by changing the bifurcation section boundary condition of one of the paths, and (b) one of the paths was partially blocked by defining a new boundary condition, i.e., wall, at the end of that branch.

To maldistribute the multiphase flow completely, more than 10,000 iterations were carried out for the perturbed condition and after that, the perturbation source was impulsively

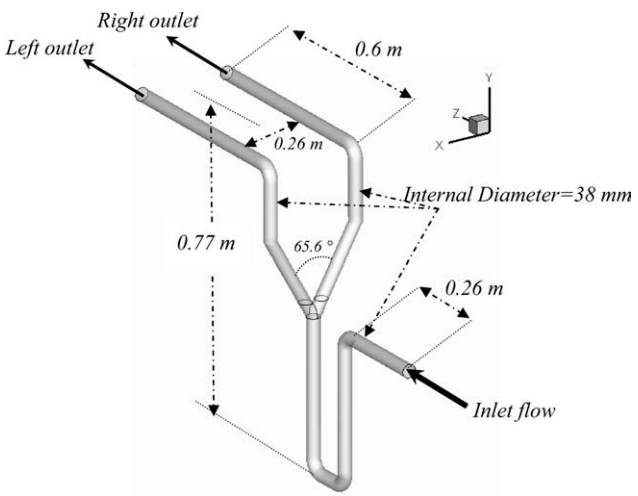

Figure 12. 3-D geometry of "Y branch" simulated by Gambit software (cross-sectional plane).

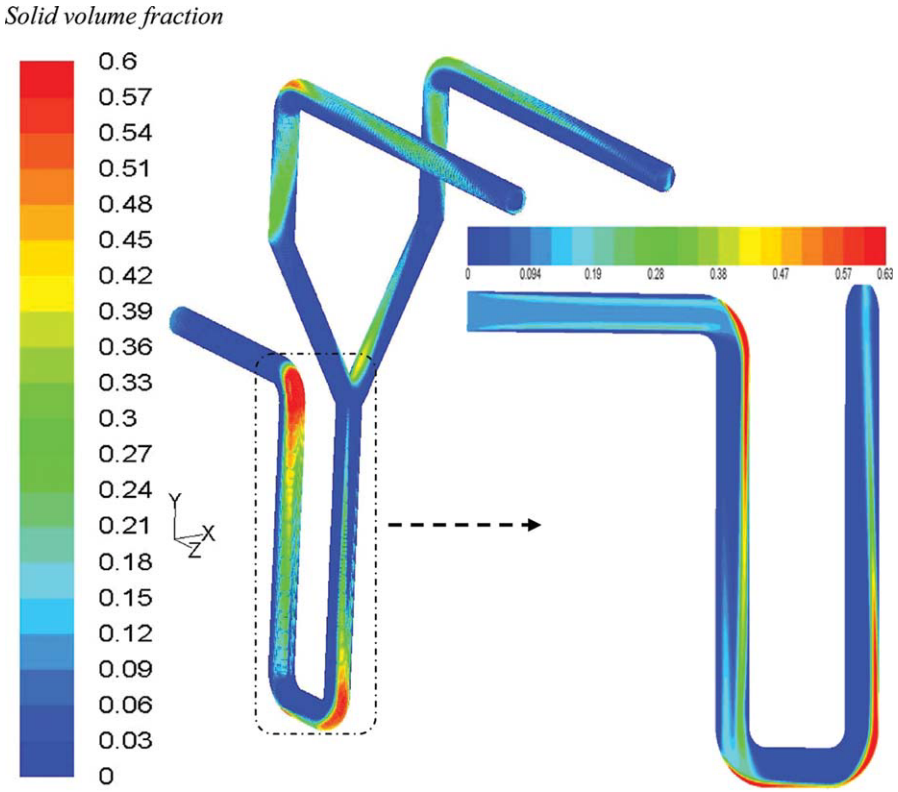

Figure 13. Steady-state contours of solid-volume fraction for 3-D simulation.

[Color figure can be viewed in the online issue, which is available at www.interscience.wiley.com.]

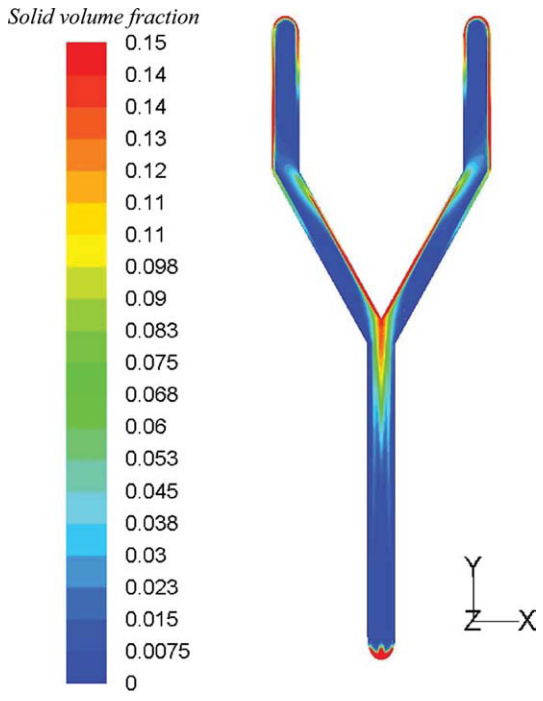

Figure 14. Steady-state contours of solid-volume fraction at bifurcation for 3-D simulation.

Middle plane view. [Color figure can be viewed in the online issue, which is available at www.interscience.wiley.com.]

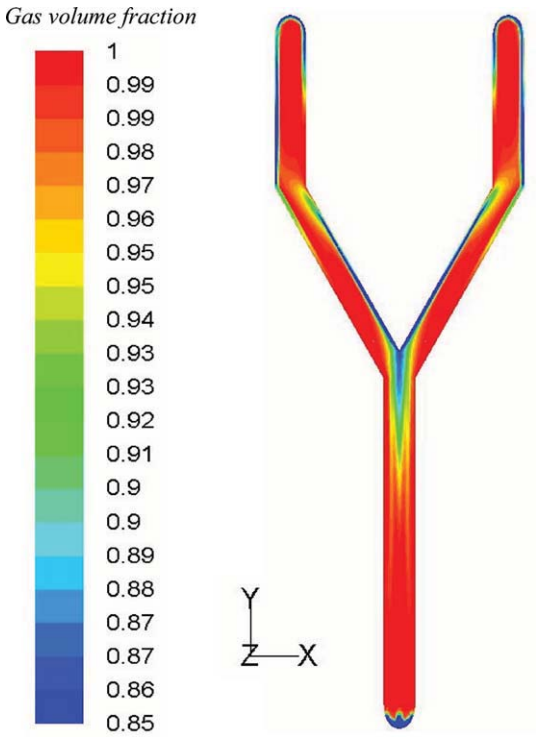

Figure 15. Steady-state contours of gas-volume fraction at bifurcation for 3-D simulation.

Middle plane view. [Color figure can be viewed in the online issue, which is available at www.interscience.wiley.com.]

removed from the system. As for the analytical stability result, it was found numerically that for both the 2-D and 3-D geometries, the stable solution was the uniform distribution solution, since, after removing the imbalance, the flow migrated to achieve an even split through the parallel paths (in 2-D case, after ~3,000 iterations is reached, while ~12,000 iterations were needed for the 3-D case).

Conclusions

Both analytical and numerical analyses suggest that the uniform distribution of gas-solid pneumatic flow through mostly-vertical identical parallel paths is the only stable solution, while maldistributed solutions are unstable. The results are consistent with energy dissipation minimization. The analysis was presented for only one gas (air at atmospheric temperature and pressure), and one particle (30 μm glass beads) at one inlet velocity 20 m/s. However, the qualitative results are likely to apply over much wider range of conditions. Therefore, it can be concluded that for the case of identical vertical parallel pipes, external\nonideal effects cause maldistribution of flow. Accurate experimental analysis combined with parallel pipe geometry is needed to confirm these predictions.

It should be emphasized that the geometry of each path may influence the flow distribution and behavior of the system. In other words, the analysis of this article applied only to vertical parallel pipes, without any additional unit (e.g., cyclone, reactor) in each path. A parallel study on the distribution of gas-solid flow through identical parallel cyclones[37] comes to different conclusions, associated with the different effects of solids loading on pressure drop.

Acknowledgments

The authors gratefully acknowledge financial support from Syncrude Canada Limited for this project.

Notation

A = cross-section area of pipe, m^2
dm_g = differential gas mass in control volume, kg
dm_s = differential solids mass in control volume, kg
dV = system differential volume, m^3
D = pipe diameter, m
f_s = solid Fanning friction factor
$f(Q_s, \varepsilon, k)$ = steady-state pressure drop across parallel paths divided by L, kg/(m^2.s^2)
f_g = gas Fanning friction factor
F = force, N
g = gravitational acceleration, m/s^2
k = coefficient in Eq. 27
L = length of pipe, m
N = number of identical parallel paths
q_s = perturbed volumetric flow rate, m^3/s
Q_{gi} = gas flow rate passing through path i, m^3/s
Q_{gt} = total inlet gas flow rate, m^3/s
Q_{si} = solids flow rate passing path i, m^3/s
Q_{st} = total inlet solids flow rate, m^3/s
Re = Reynolds number based on pipe diameter, $u_g D/\upsilon$
t = time, s
u_g = actual gas velocity in the voids or velocity of porosity wave, m/s
u_s = solid velocity, m/s
u_t = single-particle settling (or terminal) velocity in an undisturbed fluid, m/s

Greek letters

α_s = solid-volume fraction, $(1-\varepsilon)$
ΔP_i = pressure drop through path i, Pa
ρ_g = gas density, kg/m^3
ρ_s = solid density, kg/m^3
ε = voidage (volumetric void fraction)
μ = gas viscosity, kg/(m.s)
γ = fraction of gas flowing through branch 1
σ = fractions of solids flowing through branch 1
δ_s = perturbation amplitude, m^3/s
λ = eigenvalue (or growth factor), 1/s

Literature Cited

1. Stern A, Caplan K, Bush P. Parallel operation of cyclones in cyclone dust collectors. *API Dust-Collector Subcommittee*. 1955:41–43.
2. Koffman JL. The cleaning of engine air, Part 2. *Gas Oil Power*. April 1953;89–94.
3. Broodryk NJ, Shingles T. Aspects of cyclone operation in industrial chemical reactors. Preprints for Fluidization VIII Conference, Tours, France. May 14–19 1995:1083.
4. Smellie J. Notes on dust suppression and collection. *Iron Coal Trades Rev*. 1942;144(3860):169–227.
5. Hartge E-U, Budinger S, Werther J. In: *Circulating Fluidized Bed Technology VIII*. Beijing: International Academic Publishers, World Publishing Corp; 2005:675–682.
6. Shevtchenko VA, Franke W, Gummel P, Kotrus M, von Wedel G. Proceedings of 18th International Conference on Fluidized Bed Combustion; 2005; New York: ASME.: paper FBC2005-78034.
7. Wu Y, Lu J, Zhang J, Yue G, Yu L. In: *Circulating Fluidized Bed Technology VIII*. Beijing: International Academic Publishers, World Publishing Corp; 2005:529–536.
8. Kim TW, Choi JH, Shun DW, Jung B, Kim SS, Son JE, Kim SD, Grace JR. Wastage rate of waterwalls in a commercial circulating fluidized bed combustor. *Can J Chem Eng*. 2006;84:680–687.
9. Kim TW, Choi JH, Shun DW, Kim SS, Kim SD, Grace JR. Wear of water walls in a commercial circulating fluidized bed combustor with two gas exits. *Powder Technol*. 2007;178:143–150.
10. Grace JR. *Maldistribution of flow through parallel cyclones in circulating fluidized beds*. In: *Circulating Fluidized Bed Technology*. Hamburg: TuTech Innovation; 2008:969–974.
11. Flour I, Boucker M. Numerical simulation of the gas-solid flow in the furnace of a CFB cold rig with ESTETASTRID code. In: *Circulating Fluidized Bed Technology VII*. Ottawa: CSChE; 2002:467–474.
12. Yue GX, Yang HR, Nie L, Wang YZ, Zhang H. Hydrodynamics of 300MW_e and 600 MW_e CFB boilers with asymmetric cyclone layout. Hamburg: TuTech Innovation; 2008:153–158.
13. Schneider H, Frank T, Pachler DK, Bernert K. A Numerical study of the gas-particle flow in pipework and flow splitting devices of coal-fired power plant. 10th Workshop on Two-Phase Flow Predictions. Martin-Luther-Universitat Halle-Wittenberg, Halle Saale, Germany; 2002:227–236.
14. Kuan BT, Yang W. Mal-distribution of coals in lignite-fired power station mill ducts: CFD simulations and experimental validation. International Conference on Coal Science Technology; 2005; Okinawa, Japan.
15. Giddings D, Aroussi A, Pickering SJ, Mozaffari E. A 1/4 scale test facility for PF transport in power station pipelines. *Fuel*. 2004;83:2195–2204.
16. Bolthrunis CO, Silverman RW, Ferrari DC. Rocky road to commercialization: breakthroughs and challenges in the commercialization of fluidized bed reactors. In: *Fluidization XI*. Engineering Conference International: New York; 2004:547–554.
17. Boyd DT, Grace JR, Lim CJ, Adris AM. Cold modelling of an internally circulating fluidized bed membrane reactor. *Int J Chem Reactor Eng*. 2007; 5: A26.
18. Zhang L, Du W, Bi X, Wilkinson DP, Stumper J, Wang H. Gas-liquid two-phase flow distributions in parallel channels for fuel cells. *J Power Sources*. 2009;189:1023–1031.
19. Ozawa M, Akagawa K, Sakaguchi T. Flow instabilities in parallel channel flow systems of gas-liquid two-phase mixtures. *Int J Multiphase Flow*. 1989; 15:639–657.

20. Minzer U, Barnea D, Taitel Y. Flow rate distribution in evaporating parallel pipes–modeling and experimental. *Chem Eng Sci*. 2006; 61,7429–7259.
21. Grace JR, Cui H, Elnashaie SSEH. Non-Uniform distribution of two-phase flows through parallel identical paths. *Can J Chem Eng*. 2007;85:662–668.
22. Holmes T, Bradley MSA, Selves TP, Farnish RJ, Bridle I, Reed AR. Techniques for control of splitting ratios of particulate materials at bifurcations in pneumatic conveying pipelines. *Proc Inst Mech Eng*. 2000; 214, Part A: 657–667.
23. Fan L-S, Zhu C. *Principles of Gas-Solid Flows*. Cambridge: Cambridge University Press; 1998.
24. Clift R, Grace JR, Weber ME. *Bubbles, Drops, and Particles*. New York: Academic Press; 1978.
25. Marcus RD, Leung LS, Klinzing GE, Rizk F. *Pneumatic Conveying of Solids*. London: Chapman and Hall; 1990.
26. Konno H, Satio SJ. Pneumatic conveying of solid through straight pipes. *Chem Eng Jpn*. 1969;2:211.
27. Drew TB, Koo EC, McAdams WH. The friction factors for clean round pipes. *Trans AIChE J*. 1932;28:56–72.
28. Klinzing GE. *Gas Solid Transport*. New York: McGraw-Hill; 1981.
29. Govier GW, Aziz K. *The Flow of Complex Mixtures in Pipes*. New York: van Nostrand Reinhold; 1972.
30. Weber M. *Stromungs-Fordertechnik*. Mainz: Krausskopf Verlag; 1973.
31. Yang WC. International Powder and Bulk Solids Handling and Processing Conference Exposition; May 11–14, 1976; Chicago, Ill.
32. Wang Q, Squires KD, Simonin O. Large eddy simulation of turbulent gas-solid flows in a vertical channel and evaluation of second-order models. *Int J Heat Fluid Flow*. 1998;19:505–511.
33. Li J, Kwauk M. Exploring complex systems in chemical engineering-the multi-scale methodology. *Chem Eng Sci*. 2003;58:521–535.
34. Pustylnik L, Barnea D, Taitel Y. Prediction of two-phase flow distribution in parallel pipes using stability analysis. *AIChE J*. 2006; 52:3345–3352.
35. Masnadi-Shirazi MS. *Mal-Distribution of Gas-Solid Flow Through Identical Parallel Paths*. Vancouver, BC: University of British Columbia; 2009. M.A.Sc. Thesis.
36. Gidaspow D, Bezburuah R, Ding J. Hydrodynamics of circulating fluidized beds, kinetic theory approach. In: *Fluidization VII*, *Proceedings 7th Engineering Foundation Conference on Fluidization*. 1992:75–82.
37. Masnadi MS, Grace JR, Bi X, Elyasi S. Distribution of multi-phase gas-solid flow across identical parallel cyclones. *Separation and Purification Technology*. submitted for publication in 2009 (Ref. No.: SEPPUR-D-09-00917).

Manuscript received July 30, 2009, and revision received Oct. 19, 2009.